DOI: 10.1111/cgf.14349
Eurographics Symposium on Rendering 2021
A. Bousseau and M. McGuire
(Guest Editors)

Volume 40 (2021), Number 4

A combined scattering and diffraction model for elliptical hair rendering

Alexis Benamira & Sumanta Pattanaik

University of Central Florida

Figure 1: *Comparison between real life hair picture (middle) and hair renderings using our dual model (left) and current state of the art ray scattering model [CBTB16] (right). Hair fibers are placed between the viewer and a strong light source. On the real picture, we observe a strong forward scattering likely due to diffraction. Our model ($a = 30\mu m$, $b = 20\mu m$, $d_{diff} = 1$, and a melanin concentration of 8) can render a similar diffraction effect while the ray model falls short at modeling it.*

Abstract

Realistic hair rendering relies on fiber scattering models. These models are based on either ray tracing or on full wave-propagation through the hair fiber. Ray tracing can model most of the scattering phenomenon observed but misses the important effect of diffraction. Indeed human natural hair specific dimensions and geometry demands for the wave nature of light to be taken into consideration for accurate rendering. However, current full-wave model requires nonpratical, several days precomputation, that needs to be repeated for every change in the hair geometry or color, for appropriate results. We present in this paper a dual hair scattering model which considers the dual aspect of light: as a wave and as a ray. Our model accurately simulates both diffraction and scattering phenomena without requiring any precomputation. Furthermore, it can simulate light transport in hairs of arbitrary elliptical cross-sections. This new dual approach enables our model to significantly improve the appearance of rendered hair and qualitatively match scattering and diffraction effects seen in photos of real hair while adding little computation overhead.

CCS Concepts

• ***Computing methodologies*** → ***Reflectance modeling;***

1. Introduction

Light has a dual aspect since it has been experimentally characterized both as a ray and as a wave at the same time. In the field of computer graphics, we mostly consider light as a ray. It has permitted the development of very satisfactory models to render light effects for many situations since we principally work within the visible spectrum wavelength range. Indeed when the light wavelength is far inferior to the dimensions of the object it interacts with, the wave effects of the light are negligible. However this changes when light interacts with objects with dimensions closer to that of the light wavelength. In the latter settings, effects from interference

and diffraction phenomena become prominent. Hairs are interesting because they lie at the border. On the one hand, they are thick enough so that most scattering effects can be modeled with light considered as a ray. On the other hand, hairs are thin enough that light gets diffracted when interacting with them.

This diffraction creates a strong forward scattering effect that can not be modeled using classical ray reflection functions. A second key issue that needs to be addressed when considering hairs is that of the cross-section. A natural hair fiber should be modeled as a cylinder with an elliptical cross-section. The ratio of the semi-major axis over the semi-minor axis varies and may reach values of 1.6. The non-circular feature of the hair fiber cross-section is key to account for differences in hair appearance [KM17]. Current hair models either rely on heavy precomputation to model ellipticity or fall short at modeling it accurately [KM17].

To tackle both issues, we developed a new dual extension to current hair scattering model that takes into account the elliptical cross-section of the hair fiber as well as the light diffraction phenomenon. As opposed to current solutions, our model is precomputation-free, allowing easier practical usage, and integrating the dual nature -wave and ray- of light. We have integrated our model in a modern offline ray tracer and applied it to hair rendering. We measured rendering performances of our model and compared it to current classical hair model performances [CBTB16]. We also performed qualitative comparisons to underline the new effects enabled by our model.

The main contributions of our work are as follows. We provide a new precomputation-free azimuthal scattering function for hair rendering which includes:

-full derivation for light transport inside the elliptical hair fiber that supports light arriving from any angle.

-integration of a new diffraction scattering lobe, with study of spectral effects and integration.

The organization of the rest of the paper is as follows. First, we offer an overview of the state of the art in hair scattering models and wave reflection models. Then, we lay the theoretical background on which our work is based. Afterward, we describe our new dual model in two parts. One on the ray interaction with arbitrary elliptical cross-section fibers. The other on the wave diffracted by the same hair geometry. Finally, we will present our results.

2. Previous work

Hair models. In 2003, Marschner et al. [MJC*03] presented the first hair scattering model based on the scattering of a dielectric circular cylinder. The fundamental layout that they introduced will be presented in Section 3 as we also use a dielectric cylinder representation for our hair fiber. It should be noted that their initial extension to cover small elliptical cross-section settings was later shown to inaccurately reflect the difference with circular section [KM17]. Following this work, important research efforts have been undertaken to improve hair rendering models. D'Eon et al. [dFH*11], offered a new energy-conserving longitudinal scattering function, a new simple way to sample the hair scattering function [dMH13] and a new non-separable longitudinal scattering function which takes into account the azimuthal angle when computing the longitudinal function [dMH14]. To accurately model fur, Yan et al. extended the circular dielectric cylinder model by including a second cylinder concentric to the first one [YTJR15] [YJR17]. The latter model can also be used to render hair. [ZW07] formalized the notion of Bidirectional Curve Scattering Distribution Function (BCSDF) for representing the scattering distribution of a fiber in the far field approximation. BCSDF can also be used to describe textile fibers even though they often have more complex shape than hair fibers [ACG*17].

Our model finds its origin in the work of Chiang et al. [CBTB16]. Their model provides several improvements over D'Eon's [dFH*11]. It redefines the azimuthal scattering function using a logistic distribution in order to improve rendering speed and allows good artistic control over the hair aspect.

Some hair rendering models rely on precomputation to gain some efficiency [OTS10]. The efficiency they gain is at the expense of memory storage and practicability, since large tables upload is necessary. In recently published works, two groups have attempted to address both issues of ellipticity and wave effects. They used precomputation, not for efficiency's sake but rather to create more realistic models.

In 2017, [KM17] offered an extensive investigation on elliptical hair fibers. Their measurements of light scattering by real hairs concluded to the necessity of a new scattering model that would accurately account for the ellipticity of the hair fiber. In the same paper, they provided a new azimuthal scattering function that accurately matches the measurements. Unfortunately, this model relies on heavy precomputation and requires the user to load 400MB worth of precomputed tables. Their measurements also revealed a new strong forward scattering lobe that failed to be modeled by their ray tracing simulation. In their recent work, [XWM*20] presented a new full wave-based model for fiber scattering. For very thin fibers such as silk or spider web, this new model reproduces iridescence effects due to the interferences and diffractions of the light waves. For thicker fibers, this model underlines the impact of diffraction which introduces strong forward scattering of the light. This new model relies on even heavier precomputation efforts that can take up to several days and even larger data tables loading than required by [KM17]. These developments reveal the central importance of elliptical cross-section and wave effects in hair fiber scattering even though the proposed solutions are of limited practical use. Our model aims at accurately taking into account both the ellipticity of the hair fiber and the wave nature of light into a new dual scattering model which is precomputation-free and has relatively little overhead.

Wave models. The wave nature of light is attracting more attention within the rendering community in recent years. [HP17] introduced a dual model accounting for the duality of light. They presented a microfacet reflection model based on both the microscale geometry where light is considered as a ray and on the nanoscale geometry where light is considered as a wave. This new dual model better fits the scattering measurements. The proper rendering of many iridescence effects requires factoring in the wave nature of light. [YHW*18] and [WVJH17] have addressed this issue, coming up with various solutions for scratch iridescence on metallic

surfaces. [BB17] and [Ste19] have investigated the integration of spectral dependencies to reproduce proper iridescence without the use of expensive spectral rendering. The study of diffraction for surface reflection has also been adressed in [Sta99] and [CHB*12]. To the best of our knowledge, only [XWM*20] has tried to tackle the issue of rendering wave scattering effects in the setting of hair fibers.

Optics. Light scattering by ellipsoidal droplets has attracted a lot of attention in optics mainly in the study of rainbows. Although our interest lies in elliptical cylinder fibers, the scattering of light by droplets shed some insight into what can happen in the fiber case. Two general approaches have been developed. One is based on calculating the propagation of rays inside the droplet, [Loc96], [LA97]. The second relies on solving the wave propagation through the droplet [ŽD86]. Our derivation of light propagation inside the elliptical fiber generalizes the work of [LM94] to arbitrary incoming angle and multiple light bounces inside the hair. Studies of elliptical cylinder scattering can be found. Using ray propagation, [ALS98] relies on the Fourier Transform to study backward scattering caustics. Our model studies both forward and backward scattering and aims for easy integration in a rendering context. The use of wave propagation is mainly applied to antenna devices in the optics literature and relies mainly on Mathieu function [MW08], [Zou11]. However, all such studies involve large wavelength values when compared to cylinder thickness, and thus do not apply to our setting of hair fibers interacting with visible light.

3. Background

We will start by presenting the fundamental layout, resulting from previous researches in the field which forms the base of our model. All notations can be found in Table 1.

Hair rendering is based on the computation of light scattering by every single hair fiber. The scattering function in the case of a fiber is called the Bidirectional Curve Scattering Distribution Function (BCSDF) [ZW07] and named S in the equations throughout this paper. The incoming and reflected light directions are expressed in a spherical coordinate system and can be fully characterized by the longitudinal angle $\theta \in [-\pi, \pi]$ and the azimuthal angle $\phi \in [0, 2\pi]$. The situation is presented in Figure 2.

We use the factored lobe approximation [MJC*03] which assumes that the scattering function can be divided into several modes, each representing the scattering of light based on the number of time the ray travels inside the hair. Most of the light energy is scattered in the first three modes [dFH*11]. By noting p the number of times the ray is propagated through the fiber, we have:

- the R lobe ($p = 0$) describing the light immediately reflected by the fiber,

-the TT lobe ($p = 1$) describing the scattering of the light after one propagation inside the fiber,

- the TRT lobe ($p = 2$) describing the scattering of the light after two propagations inside the fiber.

In Section 4, we provide the derivation for the first three lobes for an elliptical cross-section fiber. See Figure 3 for illustration. However, should one be interested in including more lobes [dFH*11], extrapolating to higher orders of p is straightforward.

Notation	Parameter	Value
ϕ_i	Incoming azimuthal angle	$[0, 2\pi]$
$\phi_{r,p}$	Reflected azimuthal angle for lobe p	$[0, 2\pi]$
$\theta_{i/r}$	Incoming/reflected longitudinal angle	$[-\pi, \pi]$
S	BCSDF	/
p	Number of light travels inside the hair	$0, 1, 2$
h	Displacement of intersection point	$[-1, 1]$
ρ	Hair's index of refraction	1.55
s_p	Logistic scale for lobe p	/
M_p	Longitudinal scattering function for lobe p	/
N_p	Azimuthal scattering function for lobe p	/
$\mathcal{L}$	Logistic distribution	/
A_p	Energy scattered in lobe p	/
ϕ_p	Azimuthal angles difference for lobe p	/
$\eta(\theta_i, \rho)$	Bravais' index	/
a	Ellipse semi-major axis (μm)	$[50, 100]$
b	Ellipse semi-minor axis (μm)	$[50, 100]$
$D(\phi_i)$	Hair diameter	$[2b, 2a]$
$\vec{n}$	Normal vector to the ellipse	/
$\gamma_{i/t,p}$	Incident/refracted angle for lobe p	$[\frac{-\pi}{2}, \frac{\pi}{2}]$
L_p	Length of pathway p inside the hair fiber	/
$F(\rho, \theta)$	Fresnel coefficient calculation function	/
f_p	Fresnel coefficient for lobe p	$[0, 1]$
T_p	Transmission coefficient for lobe p	$[0, 1]$
σ	Absorption of the hair fiber	/
E_0	Amplitude of the incoming electic field	/
λ	Wavelength of incoming light (nm)	$[380, 780]$
Ω	Transmission function of the hair	$[0, 1]$
δ	Optical path difference	/
$\Delta\Phi$	Phase difference	/
C_{diff}	Scattering distribution for diffraction	/
F	Fresnel number	/
V	Viewer distance	/
N_{diff}	Azimuthal diffraction scattering function	/
ϕ_{diff}	Azimuthal angles difference for diffraction	/
s_{diff}	Logistic scale for diffraction	/
d_{diff}	Parameter over outer cylinder's thickness	$[0, 1]$

Table 1: *Parameters used in this work.*

$$S(\theta_r, \theta_i, \phi_r, \phi_i, h, \rho, s) = \sum_{p=0}^{\inf} S_p(\theta_r, \theta_i, \phi_{r,p}, \phi_i, h, \rho, s_p) \quad (1)$$

Following classical approximation models [MJC*03], [dFH*11], [CBTB16], we further assume that, for each mode, the scattering function can be described as the product of the longitudinal scattering function, M and the azimuthal scattering function, N.

$$S_p(\theta_r, \theta_i, \phi_{r,p}, \phi_i, h, \rho, s_p) = M_p(\theta_r, \theta_i) N_p(\theta_i, \phi_{r,p}, \phi_i, h, \rho, s_p) \quad (2)$$

For the longitudinal scattering function, we will use the energy

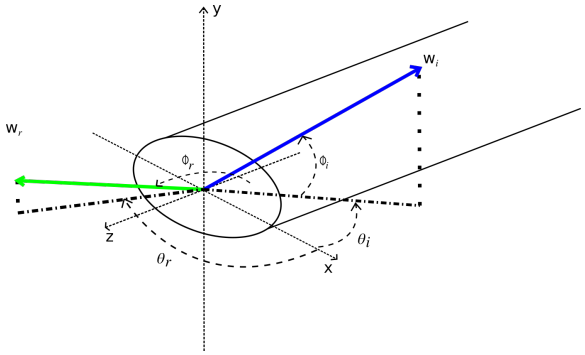

Figure 2: *Representation in spherical coordinates of the light interacting with an elliptical hair fiber. Showing the longitudinal angle* θ *and the azimuthal angle* ϕ *for the incoming ray (blue) and the reflected ray (green).*

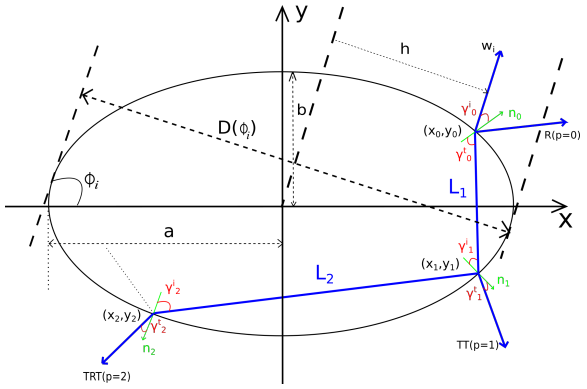

Figure 3: *Light travel path (in blue) inside the elliptical hair fiber in the azimuthal plane.*

conservation function proposed by D'Eon [dFH*11]. Based on the work of [CBTB16], we write the azimuthal scattering function in the following way:

$$N_p(\theta_i, \phi_{r,p}, \phi_i, h, \rho, s_p) = A_p(\theta_i, h, \rho)\mathcal{L}(\phi_p, s_p) \tag{3}$$

where A_p represents the amount of light being scattered in the lobe p while $\mathcal{L}$ represents the angular distribution in which the light is being scattered. We express $\mathcal{L}$ as a logistic distribution and s_p, which represents the scale of the distribution for each lobe, is computed as in [CBTB16]. N_p is expressed as a function of h representing the displacement of the intersection point between the ray and the fiber (Figure 3), ρ representing the index of refraction of the hair, and ϕ_p the difference between the incoming and reflected azimuthal angles for the lobe p.

$$\phi_p = \phi_{r,p} - \phi_i \tag{4}$$

Previous work on elliptical cross-section fibers falls short in expressing the azimuthal scattering function using those parameters and uses precomputation instead. In this work, we provide a derivation of ray propagation inside the elliptical hair fiber and thus extend the current circular cross-section scattering model of [CBTB16] to a broader, arbitrary elliptical cross-section, model.

4. Our Model - Ray Scattering

We present the first part of our dual model on ray scattering by an elliptical cross-section hair fiber. We start by introducing our assumptions which enable us to focus our work on the azimuthal scattering function N. Then we provide the derivation necessary to compute N. As expressed previously, the azimuthal scattering function can be divided into two parts. We address each part in a different subsection.

4.1. Hypotheses

The use of Bravais' index [MJC*03], allows us to consider the setting of ray-3D hair interaction problem as a two dimensional problem by projecting the incoming ray on the azimuthal plane (xy plane in Figure 2). It is done by substituting the regular index of refraction by Bravais' index when applying Snell-Descartes laws to calculate the refracted angle. We thus solely consider the azimuthal scattering function N to model the effect of elliptical cross-section and diffraction. Bravais' index varies with the longitudinal angle of the incoming ray and is computed using the following equation:

$$\eta(\theta_i, \rho) = \frac{\sqrt{\rho^2 - \sin^2(\theta_i)}}{\cos(\theta_i)} \tag{5}$$

Natural human hair thickness may vary substantially from one person to another and a value of $75\mu m$ is commonly used [Smi02]. In this work, we consider hairs as fibers of thicknesses ranging from 50 to $100\mu m$. When rendering thicker fibers, factoring in diffraction may not be necessary and for thinner fibers, interference effects have to be combined with diffraction in order to create realistic effects.

Finally, we assume that the observation distance of the camera is much greater than the width of the fiber. We will call this assumption the far field approximation. We will use it when considering the diffraction pattern introduced by the hair fiber.

4.2. Ray scattering for elliptical cross-section

We derive here the variables necessary to compute the logistic distribution for each lobe R, TT, and TRT.

We considered an elliptical hair fiber defined by a semi-minor axis length b and a semi-major axis length a. The ellipse follows the parametric equation.

$$\frac{y^2}{b^2} + \frac{x^2}{a^2} - 1 = 0 \tag{6}$$

A ray is incident on the elliptical hair fiber. The projected diameter of the hair $D(\phi_i)$ depends on the incoming azimuthal angle in the following way.

$$D(\phi_i) = 2b\cos^2(\phi_i) + 2a\sin^2(\phi_i) \tag{7}$$

The normal vector to the hair surface at any point of the surface is defined by:

$$\vec{n} = \frac{1}{\sqrt{b^4x^2 + a^4y^2}} \begin{pmatrix} b^2x \\ a^2y \end{pmatrix} \tag{8}$$

The point of intersection between the incoming ray and the hair fiber is noted (x_0, y_0). The normal at this point is noted $\vec{n_0}$. In the following section, we will derive the necessary equations to fully define the light pathway inside the elliptical hair fiber for the lobes R, TT, and TRT.

We first need to compute the incident angle of the ray on the fiber $\gamma_{i,0}$ in the following way.

$$\gamma_{i,0} = \arccos(< \vec{w_i} \cdot \vec{n_0} >) \tag{9}$$

where $< \cdot >$ is the dot product operation. The azimuthal angle for the light immediately reflected, corresponding to the R lobe, can be deduced:

$$\phi_{r,0} = \phi_i - 2\gamma_{i,0} \tag{10}$$

Rather than using the displacement of the intersection point h, the following derivation is more intuitive when considering the incident angle $\gamma_{i,0}$ directly. Thus, we will replace h by $\gamma_{i,p}$ in the following equations. We can thus define N_0 as follows

$$N_0(\theta_i, \gamma_{i,0}, \phi_i, \phi_{r,0}, \rho, s_0) = A_0(\theta_i, \gamma_{i,0}, \rho)\mathcal{L}(\phi_0, s_0) \tag{11}$$

We can then figure out the transmitted angle $\gamma_{t,0}$ using Snell-Descartes laws of refraction with Bravais' index.

$$\gamma_{t,0} = \arcsin(\eta(\theta_i, \rho)\sin(\gamma_{i,0})) \tag{12}$$

By solving the ray-ellipse intersection problem analytically, we can then express the propagation length L_1 inside the elliptical fiber by:

$$L_1 = \frac{2(b^2x_0\cos(\psi_0) + a^2y_0\sin(\psi_0))}{b^2\cos^2(\psi_0) + a^2\sin^2(\psi_0)} \tag{13}$$

with ψ_0 being equal to $\psi_0 = \phi_i - \gamma_{i,0} + \gamma_{t,0}$

Following one propagation through the hair, the ray exits at the point (x_1, y_1) where:

$$x_1 = x_0 - L_1\cos(\psi_0) \qquad y_1 = y_0 - L_1\sin(\psi_0) \tag{14}$$

We can then determine the internal incident angle and external refracted angle after one propagation through the hair fiber respectively noted $\gamma_{i,1}$ and $\gamma_{t,1}$.

The total reflected azimuthal direction for $p = 1$ is then defined by:

$$\phi_{r,1} = \phi_i - \gamma_{t,1} + \gamma_{i,1} + \gamma_{t,0} - \gamma_{i,0} + \pi \tag{15}$$

We can thus define N_1 as follows:

$$N_1(\theta_i, \gamma_{i,1}, \phi_i, \phi_{r,1}, \rho, s_1) = A_1(\theta_i, \gamma_{i,1}, \rho)\mathcal{L}(\phi_1, s_1) \tag{16}$$

Because the geometry is elliptic, total internal reflection may occur, in which case, $A_1 = 0$ and the intensity of the TT mode is null.

Proceeding in the same way as for TT mode, we can then express the propagation length L_2 inside the elliptical fiber by:

$$L_2 = \frac{2(b^2x_1\cos(\psi_1) + a^2y_1\sin(\psi_1))}{b^2\cos^2(\psi_1) + a^2\sin^2(\psi_1)} \tag{17}$$

with ψ_1 being equal to

$$\psi_1 = \arccos(< \vec{n_1} \cdot \vec{x} >) + \pi + \gamma_{i,1} \tag{18}$$

After two propagations the ray exits the hair at (x_2, y_2) obtained by:

$$x_2 = x_1 - L_2\cos(\psi_1) \qquad y_2 = y_1 - L_2\sin(\psi_1) \tag{19}$$

Internal incident angle and external refracted angle noted respectively $\gamma_{i,2}$ and $\gamma_{t,2}$ can be deduced.

The reflected azimuthal angle for $p = 2$ is defined by:

$$\phi_{r,2} = \phi_i - \gamma_{t,2} + \gamma_{i,2} + 2\gamma_{i,1} + \gamma_{t,0} - \gamma_{i,0} + 2\pi \tag{20}$$

We can thus define N_2 in the following way,

$$N_2(\theta_i, \gamma_{i,2}, \phi_i, \phi_{r,2}, \rho, s_2) = A_2(\theta_i, \gamma_{i,2}, \rho)\mathcal{L}(\phi_2, s_2) \tag{21}$$

A part of Section 7 is dedicated to the validation of this derivation. But as a first step, one can simply set the ellipse as a circle ($a = b$) to observe that we obtain the same equations as in [MJC*03], [dFH*11] and [CBTB16].

4.3. Fresnel Coefficients

Now that we have derived the variables needed to compute the logistic distribution of the scattering function, we will focus on expressing A_p representing the amount of energy being scattered for each lobe.

Let us denote $F(\rho, \theta)$ as the Fresnel coefficient calculation function, and define f_p as $f_p = F(\rho, \arccos(\cos(\theta_i)\cos(\gamma_{i,p})))$ [dFH*11]. We can thus define A_0, A_1 and A_2 in the following way:

$$\begin{aligned} A_0 &= f_0 \\ A_1 &= (1 - f_0)T_1(1 - f_1) \\ A_2 &= (1 - f_0)T_1 f_1 T_2(1 - f_2) \end{aligned} \tag{22}$$

where $T_p = \exp(-\sigma\frac{L_p}{\cos\theta})$ and σ is the absorption of the hair fiber which can be calculated from the melanin concentration in the hair [dFH*11]. As noted earlier in the elliptical cross-section case, total internal reflection may occur. Under that circumstance, the amplitude of the mode is null.

In the circular cross-section settings, we have:

$$\gamma_{i,0} = \gamma_{t,1} = \gamma_{t,2} \qquad \text{and} \qquad \gamma_{t,0} = \gamma_{i,1} = \gamma_{i,2} \tag{23}$$

Thus a general form for A_p can be written:

$$A_p = (1 - f_0)T_1^p f_1^p(1 - f_1) \quad \text{for} \quad p > 0 \tag{24}$$

In the literature, [dFH*11], another expression may be found where f_0 is used instead of f_1 in the equation above (Eq. 24). We believe that our expression is a more adequate approximation of the reflected energy since f_0 describes the energy reflected for an

incidence angle of $\gamma_{i,0}$ at an air-hair interface and f_1 describes the energy reflected for an incidence angle of $\gamma_{t,0}$ at the same interface. Internal reflection occurs with an incident angle of $\gamma_{t,0}$, thus using f_1 for the internal reflection appears more suitable. We show in Figure 4 that the difference in intensity for the TRT lobe can reach 10% by using f_1 instead of f_0.

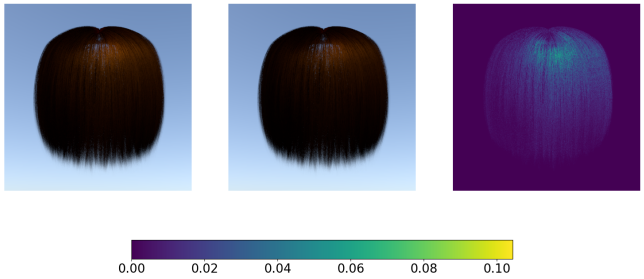

Figure 4: *A comparison of renderings of the TRT lobe of a circular hair fiber, with a melanin concentration of* 1.3*, using Eq. 24 (middle) and using an equation that replaces f_1 with f_0 in Eq. 24 (left). The intensity variation displayed on the right demonstrates that our derived expression for A_p yields a difference in intensity that can reach up to* 10%*.*

We have derived the first part of our dual model, that is the azimuthal scattering function for an arbitrary elliptical cross-section hair fiber setting with light considered as a ray. Before validating this part with numerical experiments and renderings, we will first present the second part of our dual model on diffraction by a hair fiber.

5. Our Model - Diffraction

As elucidated in Sections 1 and 2, in order to properly model the diffraction of the light by the hair fiber, we now need to consider light as a wave. Using the same setting described in Section 4.1 and illustrated in Figure 3, we now contemplate a light wave, propagating in the azimuthal plane, arriving on an elliptical cross-section fiber. We consider a linear polarization such that the electric field belongs to the azimuthal plane. We also consider that the equilibrium has been reached so there is no time variation. The electric field of the electromagnetic wave can be expressed in the following way

$$E(x,y) = E_0 \exp[\frac{-2\pi}{\lambda} i(\cos(\phi_i)x + \sin(\phi_i)y)] \tag{25}$$

5.1. Geometry modifications

To analytically solve the diffraction of the wave by the hair, we need to simplify the geometry of the problem. First, we will approximate the elliptical cross-section of the hair in the azimuthal plane by a rectangle of similar size. The width of this rectangular occlusion is equal to the projected diameter $D(\phi_i)$. We suppose it is a perfect occlusion which means that any light hitting the rectangular occlusion is blocked. The light transmission $\Omega(h)$ of the hair fiber can thus be written as follows:

$$\Omega(h) = \begin{cases} 0 & \text{if} |h| \leq \frac{D(\phi_i)}{2} \\ 1 & \text{otherwise} \end{cases} = 1 - rect_{\frac{D(\phi_i)}{2}}(h) \tag{26}$$

where h is the displacement of the intersection point.

Babinet's principle [BW19] is a powerful optical law stating that the light diffracted by an occlusion has the same distribution as the light diffracted by the exact complementary of that occlusion. Applying this principle here, we can deduce that the diffraction pattern caused by the hair is the same as the one obtained by a slit of the same size. The light wave can now be considered interacting with a rectangular slit for which the light transmission can be described by $\Omega'(h)$.

$$\Omega'(h) = \begin{cases} 1 & \text{if } |h| \leq \frac{D(\phi_i)}{2} \\ 0 & \text{otherwise} \end{cases} = rect_{\frac{D(\phi_i)}{2}}(h) \tag{27}$$

The light wave is blocked except for the part passing through a slit of the size of the hair projected diameter. An illustration of the transformation and the resulting new setting is provided Figure 5.

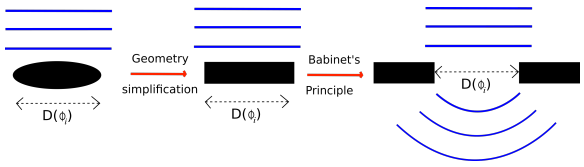

Figure 5: *Representation of the geometry modifications used to derive the diffraction scattering distribution.*

5.2. Scattered Energy derivation

We would like to express the energy of the light field seen by a viewer far away from the hair. Because we consider light as a wave, we have to sum the amplitudes and phases of the waves arriving at the viewer's position. To do so, we will calculate the difference in phase between a light wave passing through the middle of the slit and one passing through a point on the slit defined by a displacement h. The phase difference $\Delta\Phi$ can be expressed as a function of the optical path difference δ:

$$\Delta\Phi = \frac{2\pi}{\lambda}\delta \tag{28}$$

From the situation illustrated in Figure 6 we can deduct that the optical path difference is equal to :

$$\delta = h\sin(\phi) \tag{29}$$

with ϕ representing the difference between the incoming azimuthal angle and the reflected azimuthal angle.

We now sum the wave amplitudes and phases arriving at the viewer's position.

$$E_{\text{viewer}} = \int_{-\infty}^{\infty} \Omega'(h) E_0 e^{-i\Delta\Phi} dh \tag{30}$$

According to Babinet's, principle all the light waves are blocked

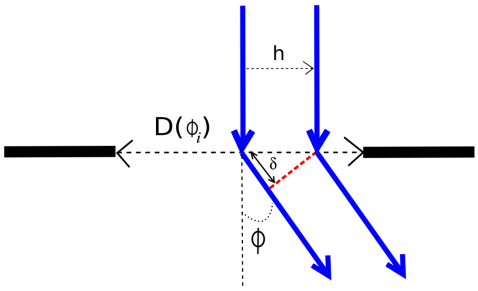

Figure 6: *Geometric representation of the optical path difference obtained with a slit of size $D(\phi_i)$.*

except for the portion passing through the slit of size $D(\phi_i)$. We can thus write the total wave as:

$$E_{\text{viewer}} = \int_{\frac{-D(\phi_i)}{2}}^{\frac{-D(\phi_i)}{2}} E_0 e^{-\frac{2i\pi}{\lambda} h \sin(\phi)} dh \tag{31}$$

Which can be analytically expressed by:

$$E_{\text{viewer}} = E_0 sinc(\frac{D(\phi_i)}{\lambda} \sin(\phi)) \tag{32}$$

with *sinc* defined as $sinc(x) = \frac{\sin(\pi x)}{\pi x}$

We derived the amplitude of the wave at the viewer's position. The energy is calculated by taking the modulus square of the amplitude. Based on this derivation, we define a new energy scattering function C_{diff} that describes the behavior of the light as a wave when interacting with the hair.

$$C_{\text{diff}} = sinc^2(\frac{D(\phi_i)}{\lambda} \sin(\phi)) \tag{33}$$

Several remarks can be made at this point. First, we used the far field approximation to obtain the diffraction distribution, also known as Fraunhofer's diffraction. To verify this assumption, we need to calculate the Fresnel number of our setting [BW19]. Indeed, the far field assumption is valid if the dimensions of the setting under study result in the value of the Fresnel number being small when compared to 1. The latter is verified under our conditions. Indeed, in our case, the Fresnel number is defined by:

$$F = \frac{D^2(\phi_i)}{V\lambda} \tag{34}$$

with V the distance of the viewer to the hair. In the worst case situation, that is the smallest wavelength light ($\lambda = 400nm$, violet) beaming through a very thick hair ($D(\phi_i) = 100\mu m$), the Fresnel number becomes larger than 1 ($F \geq 1$) when the viewer's position is $2.5cm$ away or closer from the hair. At a distance of $1m$, the F value drops almost two orders of magnitude below 1.

Next, the C_{diff} expression outcome (Eq. 33) calls for several comments. We note the dependency in λ which means that spectral rendering may be required to observe the effect in a realistic manner. We will thoroughly address this topic in the next section. Also, the variation of C_{diff} with $sin(\phi)$ should be emphasized. Since the *sinc* function is maximized at 0, the diffraction reaches a maximum when the difference in azimuthal angle between the incoming and reflected rays is equal to π. This explains the observation of a strong forward scattering lobe (see Section 7).

Lastly, the width of the *sinc* function is inversely proportional to $\frac{D(\phi_i)}{\lambda}$. This ratio is very large when considering the visible spectrum wavelength range and a natural hair thickness. Consequently, the angular spread of the diffraction scattering function is quite small. In other words, the diffraction lobe quickly falls to zero when the viewer is not in the perfect forward scattering direction.

5.3. Spectral integration and approximation

In this section, based on numerical experimentation and analysis, we will study the spectral dependency of the diffraction energy scattering function C_{diff} that we have derived in the previous section. Resorting to spectral rendering can be costly, and even though some published work provides useful techniques to reduce the cost of spectral integration [WND*14], limiting the rendering to RGB remains the less computationally expensive option.

We performed numerical spectral integration of the diffraction energy scattering C_{diff} over the visible spectrum, i.e. from $380nm$ to $780nm$. The resulting XYZ spectral integration of the diffraction distribution is shown as dotted lines in Figure 7. We fit the three blue, green, and red channels of the spectral integration with a single logistic distribution to have a single pdf to use in the rendering process, (Figure 7, solid line). The spectral integration for the red, green and blue channels are very similar to the logistic distribution for hair fibers of typical 50 to $100\mu m$ thickness range.

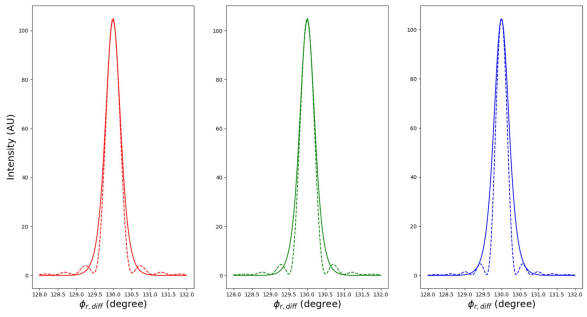

Figure 7: *Spectral integration of the diffracted energy distribution (dotted lines) as a function of the reflected azimuthal angle. Approximation by a logistic distribution is superposed in solid line for the red (left), green (middle) and blue (right) channels. The hair fiber was defined by $a = 37.5\mu m$, $b = 25\mu m$ and $\phi_i = 50^o$*

We observe that the fitting by a logistic function matches the main peak of the integral very well. However, it does smooth out the ripples. Yet this is acceptable as those ripples are only responsible for a small amount of the total energy. Based on this study, we define a new azimuthal diffraction scattering function N_{diff}.

$$N_{\text{diff}} = \mathcal{L}(\phi_i - \phi_{\text{r,diff}}, s_{\text{diff}}) \tag{35}$$

with $\phi_{\text{r,diff}} = \phi_i + \pi$

The parameter s_{diff} controls the scale of the logistic distribution. We find an expression for s_{diff} as a function of $D(\phi_i)$ that best fits the spectral integral for all values of $D(\phi_i)$ for fiber thickness between $50\mu m$ and $100\mu m$

$$s_{\text{diff}} = 2.18 * 10^5 D^2(\phi_i) - 35.82 * D(\phi_i) + 3.63 * 10^{-3} \quad (36)$$

With this, the azimuthal diffraction scattering function is fully defined. We now have all the elements of our dual scattering function. We will now describe how we implemented our model inside a ray tracing rendering engine.

6. Implementation

We implemented our new dual hair model in PBRT [PJH16]. As observed before [XWM*20], simply adding the diffraction scattering function as an extra lobe to the BCSDF (Eq. 1) leads to excessive energy being scattered by the hair. To solve this issue [XWM*20] approach relies on the precomputation of the scattered energy distribution and therefore is not applicable to our model. Instead, we propose to introduce a second concentric elliptical cylinder around the hair fiber (Figure 8).

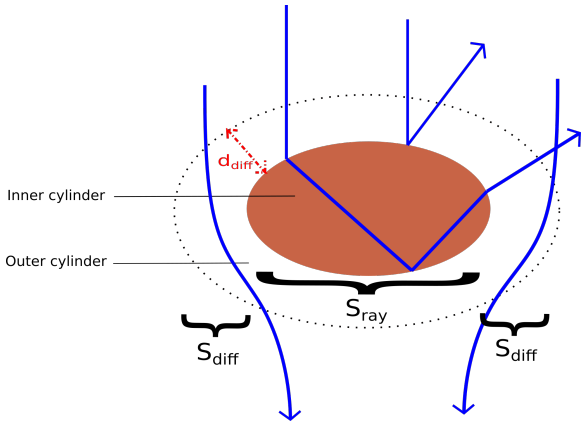

Figure 8: *A schematic of a hair fiber cross-section with our double elliptical concentric cylinder approach. Depending upon the beams' traveling paths (blue arrows), light is scattered using the ray scattering function or the diffracted scattering function.*

The inner cylinder is the actual hair fiber with its geometry unchanged. If a ray hits the inner cylinder, light is considered as a ray and the ray scattering function is calculated following the equations provided in Section 4.

$$S_{\text{ray}} = M_0 N_0 + M_1 N_1 + M_2 N_2 \quad (37)$$

If a ray intersects the outer cylinder but not the inner hair fiber, then light is considered as a wave and is diffracted. The diffracted azimuthal scattering function defined in Section 5 is then called.

$$S_{\text{diff}} = M_{\text{diff}} N_{\text{diff}} \quad (38)$$

For M_{diff} we use the longitudinal scattering function defined in [CBTB16] for $p > 2$.

The thickness of the outer cylinder is introduced as a parameter $d_{\text{diff}} \in [0,1]$ for the user to select. If $d_{\text{diff}} = 0$, then there is no outer cylinder, no light is diffracted and we have a full ray scattering model. When $d_{\text{diff}} = 1$, then the outer cylinder radius is twice that of the inner cylinder and a large amount of light is diffracted. Figure 16 illustrates the effect of the parameter d_{diff} on the final rendered image. Using this double cylinder representation, our dual model satisfies the white furnace test (see Figure 9).

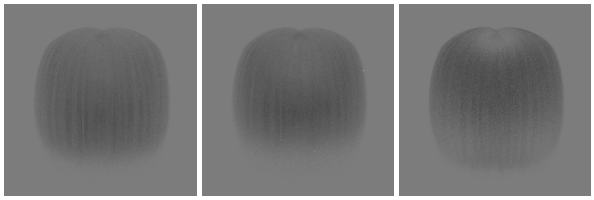

Figure 9: *White furnace test for the reference model [CBTB16] (left), and our model ($a = 37.5\mu m$, $b = 25\mu m$) without diffraction - $d_{diff} = 0$ (middle) and with diffraction - $d_{diff} = 0.4$ (right)*

We render the scenes using an Intel Xeon 64-bit 32 cores CPU. For comparison purposes, we used as a reference the model developed by [CBTB16] for ray scattering by circular cross-section hair fibers. This reference model was implemented with our Fresnel coefficient calculation presented Section 4.3. We used $50\mu m$ thick hair fibers in the scenes rendered with the reference model.

7. Results

7.1. Validation

We present here evidence that our assumptions are valid and that the dual model can qualitatively reproduce the full ray tracing simulation while offering at the same time a realistic rendering of the diffraction phenomenon. We provide a visualization of the dual scattering function (Figure 10) in the azimuthal plane and compare it with a full ray tracing simulation, used in the precomputed approach, for each term, R, TT, TRT, and the diffraction scattering function separately for better illustration and comparison. For the illustrations, we used a color scale that uses pure blue at the lower end and pure yellow at the higher end and scaled each illustration independently. For the total azimuthal scattering function, we summed all functions and we used the square root of the diffraction function to be able to visualize the other lobes as well.

We observe that our dual model provides a very good match with the ray tracing simulation for the 3 scattering lobes N_0, N_1, and N_2. Additionally, the diffraction that could not be taken into account with a ray model is now responsible for a strong scattering in the forward direction. Indeed, the two lines observed on the visualization of N_{diff} occurs when $|\phi_i - \phi_{\text{r,diff}}| = 180^o$, which is consistent with the measurements and the observations described in [XWM*20] and [KM17].

7.2. Renderings

We illustrate the significant improvements in hair renderings introduced by our new dual model described in the previous sections.

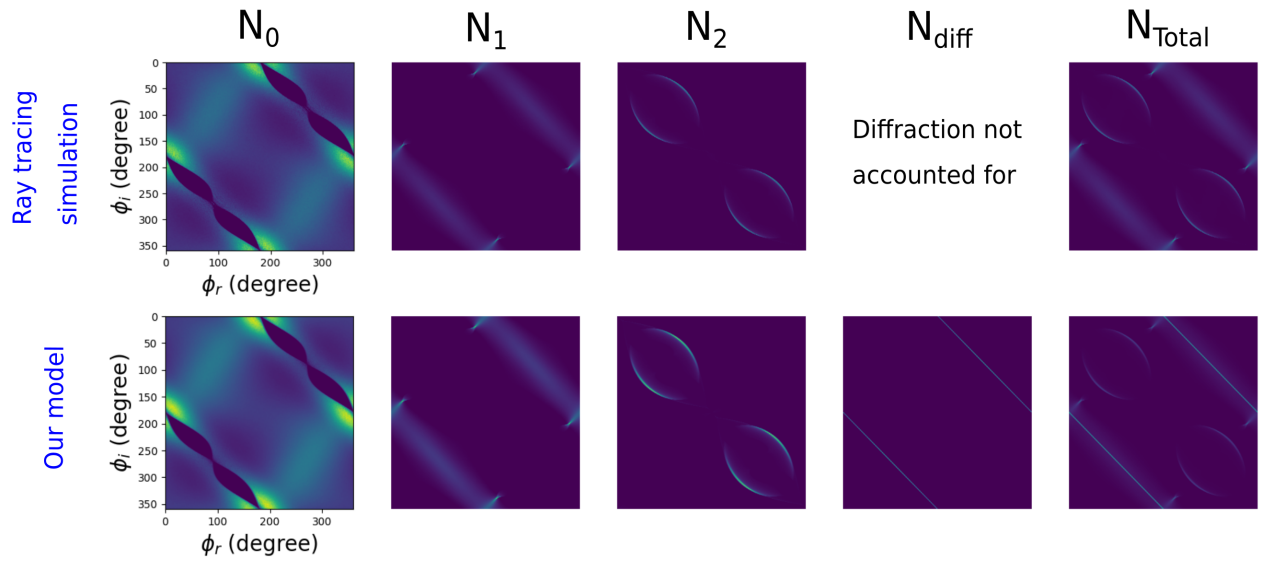

Figure 10: *Representation of the Azimuthal scattering function as a function of the incoming (ϕ_i) and reflected (ϕ_r) azimuthal angles. We compare a full ray tracing simulation, used in the precomputed approach, (top row) and our dual model (bottom row) for the three scattering lobes (N_0, N_1 and N_2 respectively), for the diffraction (N_{diff}) and the sum of the all four (N_{Total}). The hair fiber was defined by $a = 37.5\mu m$, $b = 25\mu m$, $\theta_i = 0^o$, $s = 0.01$, and a melanin concentration of 0. Our developed approach closely match the ray tracing simulation and handle the diffraction effect.*

More specifically, we rendered a few scenes that demonstrate the importance of modeling the elliptical nature of the natural hair fiber as well as the observed diffraction phenomenon resulting from accounting for the wave nature of light. All renderings have fiber elliptical cross-section semi-minor axis length b of $20\mu m$ and semi-major axis length a of $30\mu m$. Thus the average thickness of the fiber is $50\mu m$, just like the radius of the circular fibers used to render the reference model, while retaining an ellipticity of 1.5. We choose this setting such that the differences observed in the renderings will be due to the changes in the scattering distribution, not a change in the absorption of the fiber.

First, we sought to visualize the rendering contribution of modeling the hair fiber in its natural elliptical cross-section geometry. Figure 11 compares the reference model using circular cylinders with our dual model where the diffraction parameter d_{diff} is set to 0, thus voluntarily eliminating any diffraction effect. We observe a significant difference in the rendered images. More light is being scattered towards the camera when accounting for ellipticity.

The next set of renderings demonstrate the ability of the dual model to qualitatively render the observed physical diffraction phenomenon resulting from light propagating as a wave through human hair. Figure 12 illustrates again that ellipticity alone does not account for the strong forward scattering of light, so ray models can not reproduce this effect. However, as depicted when we set d_{diff} to its maximal value of 1, the rendering effect of the simulated diffraction is dramatic. Our dual model can efficiently render the strong forward scattering that can be observed in real life. In Figure 12 it can be seen that the hair fibers directly between the light and the viewer are not the only ones to get brightened by the diffraction, the fibers at the bottom of the hair geometry are brightened as well. Thus, using neutral color transparency to approximate the diffraction effect does not seem a viable option. In the setting of Figure 1 where the hair fibers are between the viewer and the light source, the strong forward scattering introduced by diffraction has a major effect on the final rendering. Adding the diffraction to the scattering model helps us to reproduce the brightening effect of the hairs observed on the real-life photograph. Because the dual model takes into account the dual behavior of light both as a ray and a wave simultaneously, it achieves realistic reproduction of hair appearance

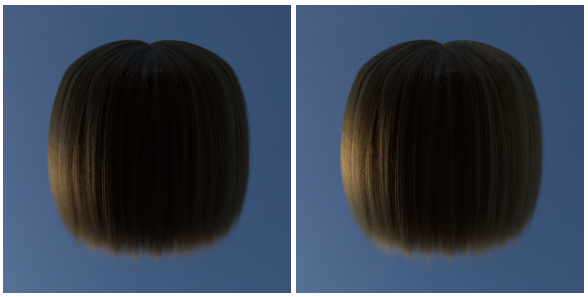

Figure 11: *Hair rendering comparison between the circular reference model (left) and our model (right) both rendered with a melanin concentration of 1. Our model was rendered using $a = 30\mu m$, $b = 20\mu m$, $d_{diff} = 0$, so no diffraction effect is displayed.*

resulting from the interaction of light with the elliptical geometry of fibers.

Figure 12: *Hair rendering comparison using the reference model (left), our model without diffraction (middle, $a = 30\mu m$, $b = 20\mu m$, and $d_{diff} = 0$), and our model with diffraction (right, $a = 30\mu m$, $b = 20\mu m$, $d_{diff} = 1$), all with a melanin concentration of 8. Ray models can not render the strong forward scattering because it is a wave effect of light. Our full model can render the diffraction which creates a great rendering enhancement.*

Our dual model can also apply to other fibers like fur. Figure 13 shows the improvements due to our dual model in the rendered bunny when compared with the rendering using the commonly used circular ray model. The strong forward scattering triggered by diffraction enables the light to propagate deeper inside the bunny's fur. One immediate consequence is that the hard shadows are considerably softened as evidenced by the fluffier appearance of the bunny's head. Moreover, the elliptical geometry of the fur fiber substantially changes the light reflections observed on the bunny's side for example. The combination of these elements provides a more natural appearance to the toy.

Even when the light source and the viewer are on the same side, our model provides some dramatic rendering effects. In Figure 14 and Figure 15, we compare two renderings obtained with the reference model and our model with diffraction ($d_{\text{diff}} = 0.2$). We observe that more light is scattered from the top of the hair and that the change in color is more smooth using our model.

In constructing our model we have set the amount of diffracted light as an adjustable parameter through the d_{diff} variable setting. It may vary from 0 (no diffraction) to 1 (maximum amount of light diffracted). We further sought to study the influence of the d_{diff} parameter on rendering. We reproduced the same scene with values of d_{diff} increasing from 0 to 1 in 0.2 increment. We can see that increasing the d_{diff} value results in the "whitening" of the general appearance of the hair fibers. The d_{diff} parameter controls the amount of light that is directly scattered by the hair from the light source. Since in this case the light source is white, the hair gets added a white contribution which results in a grayer appearance with the increase in d_{diff} value. In Figure 1 the light source is more yellow and the diffraction adds a yellow tone to the hair. As a general observation, even small values of d_{diff} (between 0.2 and 0.5) provide a good rendering of the diffraction effect.

To further demonstrate the capabilities of the model, we compared its rendering time to that of the reference ray scattering only, circular geometry model (Table 2). Very little overhead, from a few seconds to a few minutes, is observed. In addition, while offering accurate simulations of both diffraction and ray scattering

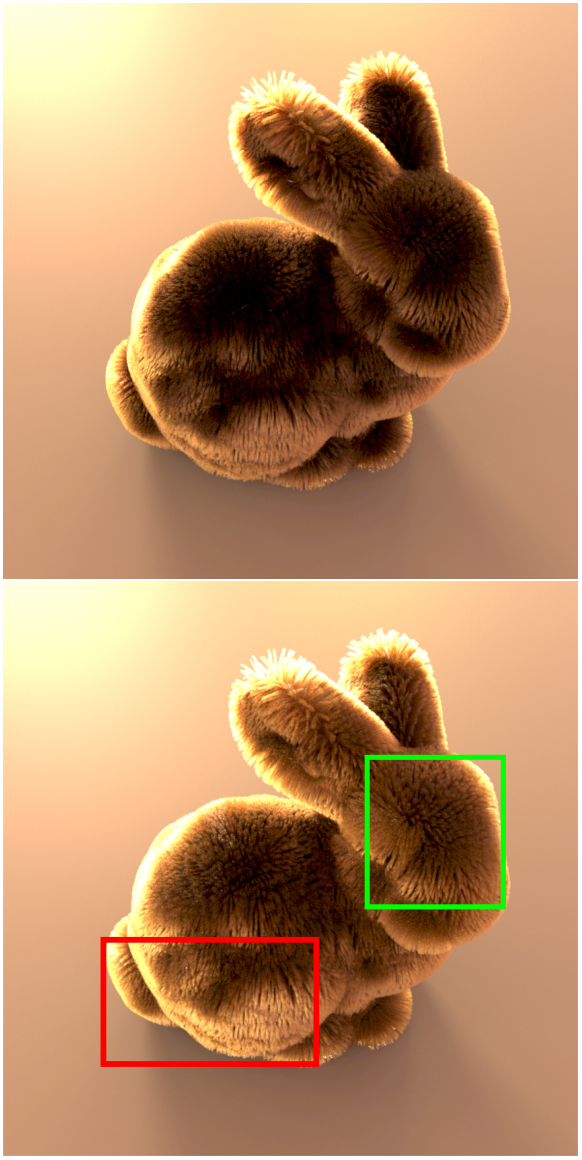

Figure 13: *Fur rendering comparison between the reference model (top) and our model (bottom) ($a = 30\mu m$, $b = 20\mu m$, $d_{diff} = 0.2$), both rendered with a melanin concentration of 1. Ellipticity modifies the reflection (red box), and diffraction smoothes the hard shadows (green box).*

phenomena for arbitrary elliptical fibers the dual model does not involve cumbersome precomputation. It can be observed that as d_{diff} increase, the rendering time increase as well. Indeed, as opposed to scattered rays, diffracted rays are not attenuated, so diffraction tends to make rays propagation longer before they are terminated. Because the rendering time is mostly driven by the ray-curve intersection computation, the more a ray propagates inside the hair geometry scene, the longer the rendering time.

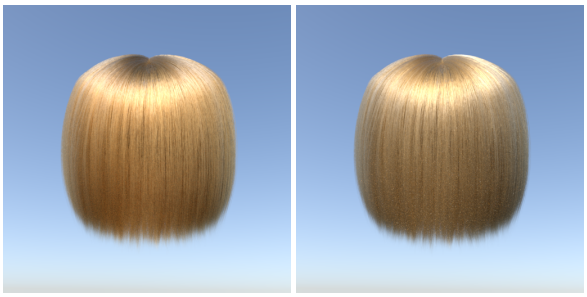

Figure 14: *Hair rendering comparison with the light source and the camera placed on the same side of the hair geometry, using the reference model (left) and our dual model (right) both rendered with a melanin concentration of* 0.3. *Our model was rendered using* $a = 30\mu m$, $b = 20\mu m$, $d_{diff} = 0.2$.

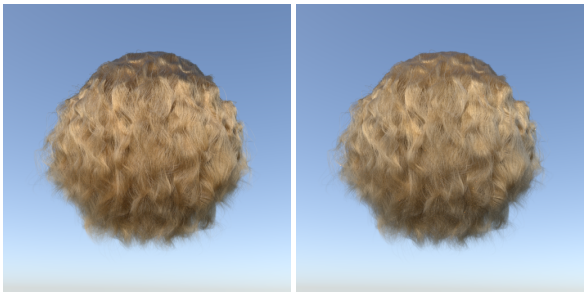

Figure 15: *Hair rendering comparison with the light source and the camera placed on the same side of the hair geometry, using the reference model (left) and our dual model (right) both rendered with a melanin concentration of* 0.3. *Our model was rendered using* $a = 30\mu m$, $b = 20\mu m$, $d_{diff} = 0.2$.

8. Limitations and future work

In this paper, we have addressed light scattering by natural human hair. Specifically, we have studied the interaction of light both as a ray and as a wave on hair fibers of thickness in the range of 50 to 100μm. Interaction with thinner fibers requires further investigations. Our model may still work for $10-50\mu m$ wide fibers with a requirement for spectral rendering of the diffraction lobe. However, when considering fibers with a few μm thicknesses, the model does not apply because the phenomenon of interference must be taken into account to accurately reproduce the appearance. The approximation of the spectral integration of C_{diff} by N_{diff} could be further investigated. For this work, we have compared the approximation of the spectral integration with a logistic distribution and a Cauchy distribution. The logistic distribution yielded better results. A thorough exploration of other distributions would be useful. Another path for further investigation includes the study of the diffraction lobe parameters d_{diff} and s_{diff} to offer better artistic control. We have set the maximum value of d_{diff} to 1 that makes the outer cylinder thickness the same as the inner cylinder radius. Finding a more physically meaningful way to set the parameter d_{diff} could also help improve our model. Finally, our model validation is mostly qualitative, real hair reflection measurements would be needed to quantitatively validate our model.

Figure	Reference model	Dual model
1	2h55	3h10
11	15m28s	16m19s
12	13m07s	13m46s
13	1h14	1h16
14	7h53	8h18
15	10h41	11h23
16	/	11h04 to 13h06

Table 2: *Rendering time for the images presented in this paper. We observe that our model introduces little overhead compare to [CBTB16].*

9. Conclusion

We have successfully introduced a new hair scattering model for rendering the human hair fibers with no precomputation requirements while still accounting for hair elliptical cross-section and light diffraction effects. The results show that our mathematical derivations of the interactions of arbitrary elliptical cross-section hairs and light taking into account its dual nature of ray and wave, qualitatively reproduces the appearance of hair as observed in real life pictures by including the diffraction phenomenon. Our model is adjustable and easily usable. We have illustrated that this dual model provides dramatic rendering enhancement of natural light effects when compared to the commonly used circular geometry and ray-only scattering models while adding very little computational overhead.

10. Acknowledgement

The first author is grateful to Panagiotis-Alexandros Bokaris and the rest of L'Oréal Research & Innovation Applied and Digital Optics team for providing him with 2020 summer internship support.

References

[ACG*17] ALIAGA C., CASTILLO C., GUTIERREZ D., OTADUY M. A., LOPEZ-MORENO J., JARABO A.: An appearance model for textile fibers. *Computer Graphics Forum 36*, 4 (2017), 35–45. doi:https://doi.org/10.1111/cgf.13222. 2

[ALS98] ADLER C. L., LOCK J. A., STONE B. R.: Rainbow scattering by a cylinder with a nearly elliptical cross section. *Appl. Opt. 37*, 9 (Mar 1998), 1540–1550. doi:10.1364/AO.37.001540. 3

[BB17] BELCOUR L., BARLA P.: A practical extension to microfacet theory for the modeling of varying iridescence. *ACM Trans. Graph. 36*, 4 (July 2017). doi:10.1145/3072959.3073620. 3

[BW19] BORN M., WOLF E.: *Principles of Optics: 60th Anniversary Edition*, 7 ed. Cambridge University Press, 2019. doi:10.1017/9781108769914. 6, 7

[CBTB16] CHIANG M. J.-Y., BITTERLI B., TAPPAN C., BURLEY B.: A practical and controllable hair and fur model for production path tracing. *Computer Graphics Forum 35*, 2 (2016), 275–283. doi:10.1111/cgf.12830. 1, 2, 3, 4, 5, 8, 11

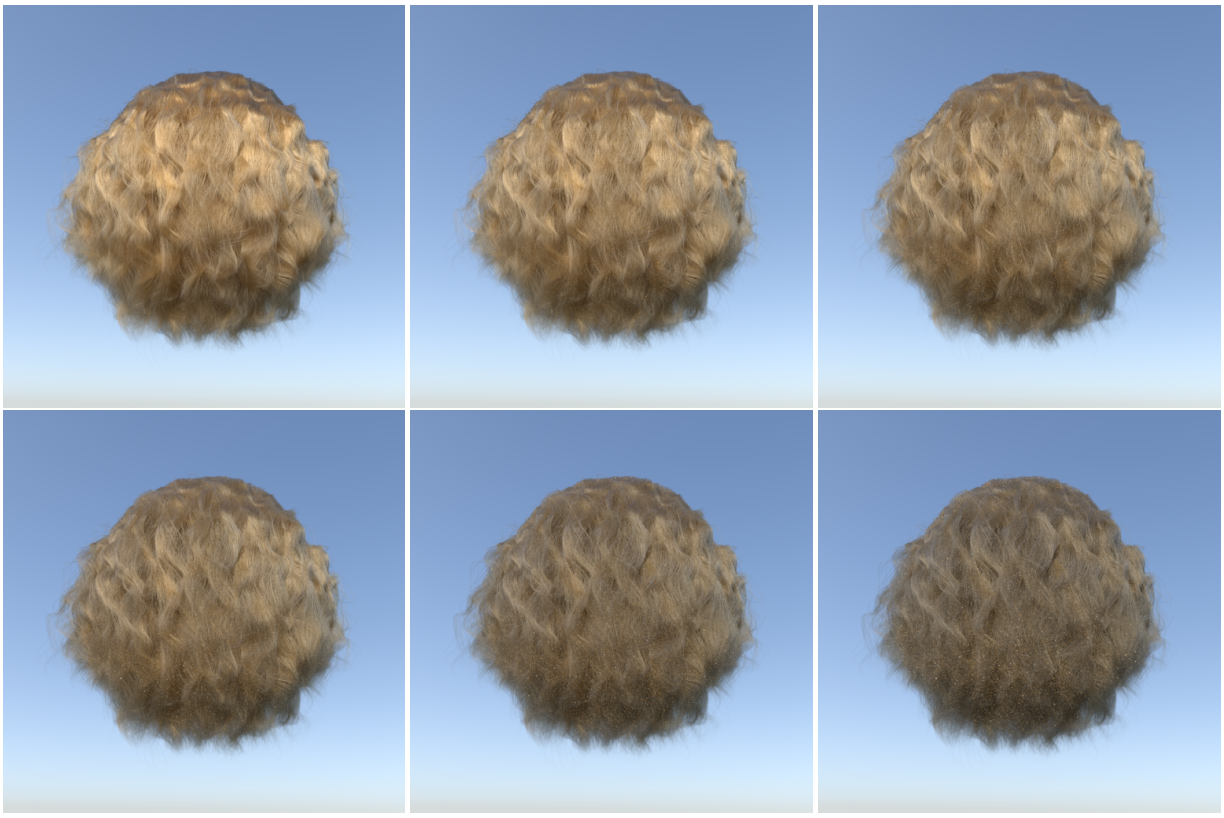

Figure 16: *Rendering of the same scene for different values of d_{diff}. top-left : $d_{diff} = 0$, top-middle : $d_{diff} = 0.2$,top-right : $d_{diff} = 0.4$, bottom-left : $d_{diff} = 0.6$, bottom-middle : $d_{diff} = 0.8$, bottom-right : $d_{diff} = 1$. The hair appearance becomes grayer as the diffraction radius increase. Other values are fixed at $a = 30\mu m$, $b = 20\mu m$, and melanin concentration of 0.3*

[CHB*12] CUYPERS T., HABER T., BEKAERT P., OH S. B., RASKAR R.: Reflectance model for diffraction. *ACM Trans. Graph. 31*, 5 (Sept. 2012). doi:10.1145/2231816.2231820. 3

[dFH*11] D'EON E., FRANCOIS G., HILL M., LETTERI J., AUBRY J.-M.: An energy-conserving hair reflectance model. In *Proceedings of the Twenty-Second Eurographics Conference on Rendering* (Goslar, DEU, 2011), EGSR '11, Eurographics Association, p. 1181–1187. doi:10.1111/j.1467-8659.2011.01976.x. 2, 3, 4, 5

[dMH13] D'EON E., MARSCHNER S., HANIKA J.: Importance sampling for physically-based hair fiber models. In *SIGGRAPH Asia 2013 Technical Briefs* (New York, NY, USA, 2013), SA '13, Association for Computing Machinery. doi:10.1145/2542355.2542386. 2

[dMH14] D'EON E., MARSCHNER S., HANIKA J.: A fiber scattering model with non-separable lobes. In *ACM SIGGRAPH 2014 Talks* (New York, NY, USA, 2014), SIGGRAPH '14, Association for Computing Machinery. doi:10.1145/2614106.2614161. 2

[HP17] HOLZSCHUCH N., PACANOWSKI R.: A two-scale microfacet reflectance model combining reflection and diffraction. *ACM Trans. Graph. 36*, 4 (July 2017). doi:10.1145/3072959.3073621. 2

[KM17] KHUNGURN P., MARSCHNER S.: Azimuthal scattering from elliptical hair fibers. *ACM Trans. Graph. 36*, 2 (Apr. 2017). doi:10.1145/2998578. 2, 8

[LA97] LOCK J. A., ADLER C. L.: Debye-series analysis of the first-order rainbow produced in scattering of a diagonally incident plane wave by a circular cylinder. *J. Opt. Soc. Am. A 14*, 6 (Jun 1997), 1316–1328. doi:10.1364/JOSAA.14.001316. 3

[LM94] LOCK J. A., MCCOLLUM T. A.: Further thoughts on newton's zero-order rainbow. *American Journal of Physics 62* (1994), 1082–1089. doi:10.1119/1.17665. 3

[Loc96] LOCK J. A.: Ray scattering by an arbitrarily oriented spheroid. ii. transmission and cross-polarization effects. *Appl. Opt. 35*, 3 (Jan 1996), 515–531. doi:10.1364/AO.35.000515. 3

[MJC*03] MARSCHNER S. R., JENSEN H. W., CAMMARANO M., WORLEY S., HANRAHAN P.: Light scattering from human hair fibers. *ACM Trans. Graph. 22*, 3 (July 2003), 780–791. doi:10.1145/882262.882345. 2, 3, 4, 5

[MW08] MAO S.-C., WU Z.-S.: Scattering by an infinite homogenous anisotropic elliptic cylinder in terms of mathieu functions and fourier series. *J. Opt. Soc. Am. A 25*, 12 (Dec 2008), 2925–2931. doi:10.1364/JOSAA.25.002925. 3

[OTS10] OGAKI S., TOKUYOSHI Y., SCHOELLHAMMER S.: An empirical fur shader. In *ACM SIGGRAPH ASIA 2010 Sketches* (New York, NY, USA, 2010), SA '10, Association for Computing Machinery. doi:10.1145/1899950.1899966. 2

[PJH16] PHARR M., JAKOB W., HUMPHREYS G.: *Physically based rendering: From theory to implementation*. Morgan Kaufmann, 2016. 8

[Smi02] SMITH G. T.: *Industrial metrology: surfaces and roundness*. Springer Science & Business Media, 2002. 4

[Sta99] STAM J.: Diffraction shaders. In *Proceedings of the 26th Annual Conference on Computer Graphics and Interactive Techniques* (USA, 1999), SIGGRAPH '99, ACM Press/Addison-Wesley Publishing Co., p. 101–110. doi:10.1145/311535.311546. 3

[Ste19] STEINBERG S.: Analytic spectral integration of birefringence-induced iridescence. *Computer Graphics Forum 38*, 4 (jul 2019), 97–110. doi:10.1111/cgf.13774. 3

[WND*14] WILKIE A., NAWAZ S., DROSKE M., WEIDLICH A., HANIKA J.: Hero wavelength spectral sampling. In *Proceedings of the 25th Eurographics Symposium on Rendering* (Goslar, DEU, 2014), EGSR '14, Eurographics Association, p. 123–131. doi:10.1111/cgf.12419. 7

[WVJH17] WERNER S., VELINOV Z., JAKOB W., HULLIN M. B.: Scratch iridescence: Wave-optical rendering of diffractive surface structure. *ACM Trans. Graph. 36*, 6 (Nov. 2017). doi:10.1145/3130800.3130840. 2

[XWM*20] XIA M. M., WALTER B., MICHIELSSEN E., BINDEL D., MARSCHNER S.: A wave optics based fiber scattering model. *ACM Trans. Graph. 39*, 6 (Nov. 2020). doi:10.1145/3414685.3417841. 2, 3, 8

[YHW*18] YAN L.-Q., HAŠAN M., WALTER B., MARSCHNER S., RAMAMOORTHI R.: Rendering specular microgeometry with wave optics. *ACM Trans. Graph. 37*, 4 (July 2018). doi:10.1145/3197517.3201351. 2

[YJR17] YAN L.-Q., JENSEN H. W., RAMAMOORTHI R.: An efficient and practical near and far field fur reflectance model. *ACM Trans. Graph. 36*, 4 (July 2017). doi:10.1145/3072959.3073600. 2

[YTJR15] YAN L.-Q., TSENG C.-W., JENSEN H. W., RAMAMOORTHI R.: Physically-accurate fur reflectance: Modeling, measurement and rendering. *ACM Trans. Graph. 34*, 6 (Oct. 2015). doi:10.1145/2816795.2818080. 2

[ŽD86] ŽUMER S., DOANE J.: Light scattering from a small nematic droplet. *Physical Review A 34*, 4 (1986), 3373. doi:10.1103/physreva.34.3373. 3

[Zou11] ZOUROS G. P.: Electromagnetic plane wave scattering by arbitrarily oriented elliptical dielectric cylinders. *J. Opt. Soc. Am. A 28*, 11 (Nov 2011), 2376–2384. doi:10.1364/JOSAA.28.002376. 3

[ZW07] ZINKE A., WEBER A.: Light scattering from filaments. *IEEE Transactions on Visualization and Computer Graphics 13*, 2 (2007), 342–356. doi:10.1109/TVCG.2007.43. 2, 3